Available online at www.sciencedirect.com
ScienceDirect
Proceedings of the Combustion Institute 000 (2022) 1–9
Proceedings of the Combustion Institute
www.elsevier.com/locate/proci

Experimental and kinetic modeling study of α-methylnaphthalene laminar flame speeds

Andrea Nobili [a], Luna Pratali Maffei [a], Matteo Pelucchi [a,*], Marco Mehl [a], Alessio Frassoldati [a], Andrea Comandini [b], Nabiha Chaumeix [b]

[a] *CRECK Modeling Lab, Department of Chemistry, Materials and Chemical Engineering "G. Natta", Politecnico di Milano, P.zza Leonardo da Vinci 32, Milano 20133, Italy*
[b] *ICARE, CNRS-INSIS, Orléans, France*

Received 5 January 2022; accepted 3 August 2022
Available online xxx

Abstract

α-Methylnaphthalene (AMN) is the primary reference bicyclic aromatic compound of diesel, and it is commonly used as a component of diesel, kerosene and jet-fuel surrogates formulated to describe real fuel combustion kinetics. However, few experimental data on neat AMN combustion are available in the literature. This work provides the first measurements of laminar flame speed profiles of AMN/air mixtures at 1 bar varying the initial temperature from 425 to 484 K, and equivalence ratio (φ) between 0.8 and 1.35 paving the way for the kinetic study of AMN combustion chemistry at high temperatures (>1800 K). The experimental data obtained in a spherical reactor are compared with kinetic model simulations. Specifically, the AMN kinetics is implemented from its analogous monocyclic aromatic compound, i.e., toluene, through the analogy and rate rule approach. This method allows to develop kinetic mechanisms of large species from the kinetics of smaller ones characterized by analogous chemical features, namely the aromaticity and the methyl functionality in the case of toluene and AMN. In doing so, it is possible to overcome the need of high-level electronic structure calculations for the evaluation of rate constants, as their computational cost increases exponentially with the number of heavy atoms of the selected species. To assess the validity of this approach, ab initio calculations are performed to derive the rate constants of the H-atom abstraction reactions by H, OH and CH_3 radicals from both toluene and AMN. The kinetic model obtained satisfactorily agrees with the measured laminar flame speed profiles. Sensitivity and flux analyses are performed to investigate similarities and differences between the main reaction channels of toluene and AMN combustion, with the former leading to ~6 cm/s faster flame speed at almost identical conditions (P=1 bar, T~425 K), as evidenced by both kinetic model simulations and experimental findings.

Keywords: Methylnaphthalene; Laminar flame speed; Rate rules; Analogy rules

* Corresponding author.
E-mail address: matteo.pelucchi@polimi.it (M. Pelucchi).

https://doi.org/10.1016/j.proci.2022.08.017

1. Introduction

The understanding of real fuel combustion chemistry in engines is of relevance in the context of climate change mitigation. This is particularly true in the challenging decarbonize process sectors such as heavy-duty road transport, aviation and maritime transport. However, the development of dedicated detailed kinetic mechanisms is hampered by the huge number of compounds that constitute real fuels and that interconnect through a complex network of reactions determining ignition, flame propagation and the formation of pollutants such as NOx, unburned species and particulate matter. Hence in the last decades kinetic modeling occurred mostly via the formulation of surrogate fuels, made of only few reference species able to reproduce physical and/or chemical properties of the real fuels [1,2].

In this context, α-methylnaphthalene (AMN) represent one of the major components of diesel [3], kerosene and alternative jet-fuel surrogates [4,5]. In the experimental and theoretical study of Ramirez et al. [3] a very similar reactivity between commercial diesel and a diesel surrogate fuel constituted by a simple AMN/n-decane mixture was observed. Violi et al. [4] used AMN as representative of the diaromatic species in the blend of a six-component mixture formulated to reproduce the distillation and compositional properties of a JP-8 aviation fuel. AMN was also included in the seven-component mixtures developed by Kathrotia et al. [5] to model 26 jet fuels and to investigate the influence on the formation of soot precursors of different chemical classes of compounds, i.e., n-paraffins, iso-paraffins, cyclo-alkanes, aromatics. However, despite the fact that AMN represents the primary reference bicyclic aromatic compound of diesel fuels with a null cetane number [3] as well as a key precursor of larger polycyclic aromatic hydrocarbons (PAHs) and soot [6], only few experimental and modeling studies focusing on neat AMN combustion are available in the literature [3,7–10].

In this work, we measured laminar flame speeds (LFS) of AMN/air mixtures in a spherical vessel at 1 bar and at three unburned gas temperatures (T_{in}=425 K, 445 K, 484 K). To the best of our knowledge, these are the first measurements of AMN/air laminar flame speeds available in the literature, while previous experiments only focused on speciation [3] and autoignition properties [7]–[8]. Then, AMN reactivity was modeled and updated in the CRECK kinetic mechanism by applying analogy and systematically extending reaction classes and rate rules from toluene, being the monocyclic aromatic counterpart of AMN, thus featuring strong chemical similarity. Specifically, H-atom abstraction reactions by H, OH and CH_3 radicals from both the methyl group and the aromatic rings of AMN and toluene were computed based on abinitio calculations to validate the kinetic assumptions adopted herein. Additional oxidation pathways were derived entirely by analogy describing the evolution of similar chemical species coherently with toluene. The kinetic mechanism thus obtained satisfactorily predicts measured laminar flame speeds. Sensitivity and flux analyses were performed to assess key reactions and chemical pathways involved in AMN combustion at the conditions investigated, and to highlight the robustness of the analogy approach adopted.

2. Methods

2.1. Experimental setup

The laminar flame speeds were measured in a spherical vessel of 56 L (i.d. 48 cm) equipped with optical access through 4 quartz opposite windows (100 mm optical diameter, 50 mm thickness). The vessel was maintained at a homogeneous temperature by means of a circulating thermal heating fluid and insulation. In the present study, the initial temperature (T_{in}) was varied (425±1 K, 445±1 K, and 484±1 K), with equivalence ratio ranging from 0.8 to 1.35, while the initial pressure in the spherical bomb was fixed to 1 bar. The minimum and maximum flame radius vary from 10 mm to 14 mm (to avoid influences on the ignition event) and from 37 mm to 46 mm depending on the flame ideality, respectively.

A Z-type Schlieren set-up coupled with a high-speed camera (Phantom v1610, 25000 frames per second acquisition rate) was used for visualization and recording of the expanding flames, while the pressure time histories were measured with a piezoelectric pressure transducer (Kistler 601A coupled to a Kistler Type 5011B Charge Amplifier). Examples of images for an α-methylnaphthalene propagating flame at φ=1.1 and T_{in}=445 K are presented in the left top panel of Fig. 1. The left bottom panel shows the corresponding pressure profile. In particular, the pressure signals were used to verify that the measurements were performed at nearly constant pressure conditions. An average increase of 0.7% in the pressure profiles was observed between the initial time and the time of the last recorded images. The images were then processed to obtain the flame radius as a function of time (Canny method), from which the adiabatic unstretched gas speed of the burned gases relative to the flame could be derived by solving the non-linear Equation S1 reported in the Supplementary Material (SM). The unstretched laminar flame speed of the unburned gases was finally obtained from the continuity equation. The average estimated errors in the three sets at T_{in}= 425 K, 445 K, and 484 K are 0.7 cm/s, 0.8 cm/s, and 1.0 cm/s, respectively, based on the uncertainty in the determination of the radii (±1 pixel). Finally, the radiation-correction terms calculated based on the equation proposed by Yu

Please cite this article as: A. Nobili, L. Pratali Maffei, M. Pelucchi et al., Experimental and kinetic modeling study of α-methylnaphthalene laminar flame speeds, Proceedings of the Combustion Institute, https://doi.org/10.1016/j.proci.2022.08.017

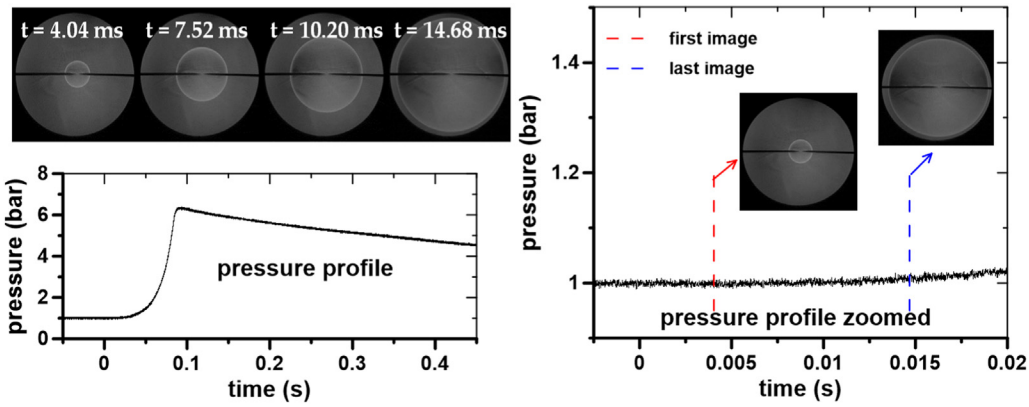

Fig. 1. α-methylnaphthalene/air flame propagation at φ=1.1, T_{in}=445 K, P_{in}=1 bar (top left panel) with the corresponding pressure profile (bottom left panel). The pressure profile between 4.04 and 12.04 ms is zoomed in the right panel.

et al. [11] is on average equal to 0.68 cm/s, 0.70 cm/s, and 0.75 cm/s for T_{in}=425 K, 445 K, and 484 K, respectively.

The reactant mixtures were prepared directly inside the vessel using the partial pressure method The partial pressures were measured with two capacitive manometers (MKS Baratron Type 631, accuracy 0.5%) of different full scales (100 Torrs and 1000 Torrs). Based on the precision of the capacitive manometers, the uncertainty in the equivalence ratio (φ) is around 1%. All the experiments were performed using laboratory dry air (0.209 O_2+0.791 N_2), while two different AMN samples, i.e., by Alfa Aesar (97% purity) and Acros Organics (98% purity) were considered in order to assess the influence of the corresponding impurities on the laminar flame speed measurements. In particular, the AMN from Alfa Aesar contains considerable amounts of methyl-substituted thiophenes while the AMN from Acros Organics contains hydrogenated impurities. Details of the two fuel samples are reported in Fig. S1 of SM. Only a slight shift was observed in the flame speed profiles obtained with the two different mixtures at 484 K (Fig. S2), with a maximum discrepancy of 0.8 cm/s on the fuel rich side. Therefore, the presence of different impurities in the fuel samples did not significantly influence the laminar flame speed measurements.

The experiments performed at T_{in}=484 K were also used to assess the repeatability of the experimental data due to errors in the determination of the flame radii. In particular, the experiments at three different equivalence ratios, φ~0.80, 1.07, and 1.35, were repeated three times each and the related results are reported in Fig. S7 of SM. The variation in the measured laminar flame speed at each φ is much lower than the corresponding experimental errors. Thus, it was possible to assume that the uncertainties due to the raw data treatment were conservative estimates of the errors. The Markstein lengths were also estimated, and an excellent repeatability of the measurements was observed. Further details of the experimental apparatus have been reported in previous publications [12,13]. Experimental data are provided in tabular form in the SM.

2.2. Kinetic mechanism

From the modeling standpoint, the aim of this work is to update the AMN chemistry within the CRECK gas-phase kinetic mechanism [14] by applying analogy and rate rules from toluene. This approach is motivated by the fact that the development of a detailed kinetic mechanism for AMN combustion entirely based on high-level theoretical calculations is inhibited by: i) the exponential increase of intermediates and related isomers involved in PAH chemistry compared to those participating to MAH chemistry [15]; ii) the high computational cost of electronic structure calculations for PAHs preventing the straightforward use of state-of-the-art theoretical methodologies recently applied to MAH chemistry [16,17].

Hence, in order to prove the validity of the analogy discussed in Section 2.2.2, we also computed rate constants for H-atom abstraction reactions by H, OH and CH_3, at the same level of theory for both toluene and AMN. The selected radicals are abstracting species involved in MAHs pyrolysis and combustion [14,18].

2.2.1. H-atom abstraction rate constant calculations

The rate constants of H-atom abstraction reactions were calculated through Ab Initio Transition State Theory based Master Equation methods (AI-TST-ME [19]), as implemented in EStokTP [20]. EstokTP automatize routines employ Gaussian G09 [21] and Molpro 2021 [22] for electronic

Please cite this article as: A. Nobili, L. Pratali Maffei, M. Pelucchi et al., Experimental and kinetic modeling study of α-methylnaphthalene laminar flame speeds, Proceedings of the Combustion Institute, https://doi.org/10.1016/j.proci.2022.08.017

structure and MESS [23] for rate constant calculations. Geometries and frequencies of the stationary points on the potential energy surface (PES) were calculated with the M06-2X functional using 6-311+g(d,p) basis set [24]. This methodology already proved accurate in the calculation of the rate constants for H-atom abstraction reactions from toluene [14]. In this respect, it is noted that the rate constant of the H-atom abstraction by OH was already reported in our previous work on toluene [14]. The energies of the stationary points on toluene PESs were refined at the CCSD(T)/aug-cc-pVTZ level of theory [25,26], and corrected for basis set size effects with the change between density fitted (DF) MP2 with aug-cc-pVQZ and aug-cc-pVTZ basis sets, as described in [25]. The resulting energy barriers estimated at M06-2X/6-311+g(d,p) and at CCSD(T)/CBS levels of theory differ by about 1-2 kcal/mol. Hence, the DFT energy barriers of the H-atom abstractions from AMN were corrected according to the difference between the CCSD(T) and DFT calculations of the corresponding TS in toluene. This approach already proved successful in the estimation of energy barriers for MAHs within the same reaction class [17].

Internal rotations were treated with the one-dimensional hindered rotor models, and the torsional potential was determined with 20° interval scans at the same level of theory used for geometry optimization. Van der Waals wells that precede and follow the TSs were also determined (as in [14]), so as to compute properly the energy barrier for quantum tunneling corrections with the Eckart model [27]. Rate constants were determined in the 500–2000 K temperature range using microcanonical variational transition state theory (VTST), as implemented in MESS [23]. Input files for the master equation calculations are available as supplementary materials.

The calculated rate constants are reported in Fig. 2.

Fig. 2a shows that very similar values were obtained for toluene and AMN in the case of H and CH_3 radicals abstracting from the methyl group, with an average discrepancy of only 22%. On the contrary, the H-atom abstraction by OH from toluene methyl group is larger than that from AMN by a factor of up to 1.5. This is due to the higher rotational barriers associated with the torsions of the OH and CH_3-OH groups related to the larger steric hindrance and the interaction with the second aromatic ring. The maxima for the hindered rotation of these groups were found to be 7 and 2 kcal/mol in AMN, while 3 and 1 kcal/mol in toluene, respectively. It is also noted that the structures of the two TSs are slightly different, with the OH tilted towards the second aromatic ring in AMN and perpendicular to the plane in toluene. This might increase the error in the correction in the energy barriers calculated at the DFT level of theory. The H-atom abstractions from the ortho site of the aromatic rings, i.e., the most reactive site, were found to be systematically faster in toluene than in AMN (factor of ∼1.5 on average), in the whole temperature range of interest (Fig. 2b). Because of the vicinity of the ortho site to the methyl group, a similar theoretical explanation for the decrease in the rate constant applies (i.e., higher steric hindrance and torsional barriers).

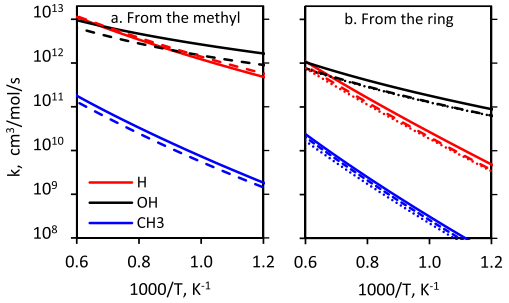

Fig. 2. Per H-atom basis H-atom abstraction rate constant by H, OH, CH_3 from a) the methyl group and b) the ortho-site of the aromatic rings of toluene (solid lines) and AMN (dashed lines). Dotted lines in b) represent the rate constnt computed by applying the rate rule.

2.2.2. *Analogy and rate rules from toluene kinetics*

The analogy and rate rules approach widely used in the literature [28] was adopted to develop the AMN model from that of toluene, recently revised in the CRECK kinetic framework based on theoretical determination of rate constants [14]. The analogy and rate rule approach assumes that chemical species with the same functional groups feature similar reactivity. This assumption was successfully used to describe the pyrolysis and combustion kinetics of different classes of chemical species, such as n-alkanes [29], phenolic [30] and aromatic species [17]. Moreover, H-atom abstraction rate constants discussed in Section 2.2.1 provided an additional reliable theoretical reference for the application of such rules.

Based on analogy rules, all the rate constants of H-atom abstraction reactions from the methyl functional group of AMN were assumed to be equal to those of toluene. The theoretical findings reported in Fig. 2a support this approach, except from the rate constants of the H-atom abstraction by OH from AMN. Hence, this rate constant was implemented directly from the theoretical calculations due to the significant difference with its reference rate constant. On the other hand, following the rate rule approach [28], all the rate constants of H-atom abstraction reactions per site from the aromatic rings of AMN were reduced to 7/10 of the corresponding rate constants of toluene. This scaling factor stems from the different number of

Please cite this article as: A. Nobili, L. Pratali Maffei, M. Pelucchi et al., Experimental and kinetic modeling study of α-methylnaphthalene laminar flame speeds, Proceedings of the Combustion Institute, https://doi.org/10.1016/j.proci.2022.08.017

Table 1
List of reaction with pre-exponential factor A of the Arrhenius law tailored from toluene kinetics.

Reaction	$A_{AMN}/A_{TOLUENE}$
$H+C_{10}H_7CH_3=H_2+C_{10}H_6CH_3$	7/10[a]
$OH+C_{10}H_7CH_3=H_2O+C_{10}H_7CH_2$	1/1.5[b]
$O+C_{10}H_7CH_3=H+CH_3C_{10}H_6O$	7/10[a]
$2C_{10}H_7CH_2=>BINs$	1/4[c]
$C_{10}H_7CH_2+C_{10}H_7CH_3=>H+BINs$[d]	1/4[c]
$2C_{10}H_6CH_3=>H_2+BINs$	1/4[c]
$C_{10}H_6CH_3+C_{10}H_7CH_3=>H+BINs$	1/4[c]

[a] Based on the rate rule. Same scaling applied to all the H-atom abstraction and ipso-addition reactions occurring on each site in the aromatic ring of AMN [b]From theoretical calculations (Fig. 2a). [c]Based on symmetry considerations. [d]BINs represent lumped pseudo species describing large PAHs and carbonaceous particles in the soot model [31] coupled with the gas-phase kinetics.

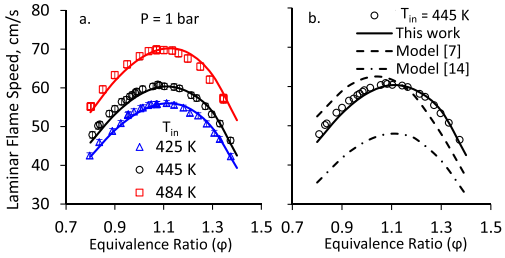

Fig. 3. (a) Laminar flame speeds of an AMN/air mixture at P=1 bar varying the initial temperature T_{in}. Error bars, with a maximum of ±1 cm/s are also reported. (b) Comparison between LFS measured and computed in this work with those obtained with other literature models [7,14].

H atoms as well as from the systematic reduction of the rate constant obtained from theoretical calculations. The rate constants thus obtained for the H-atom abstraction by H, OH and CH_3 radicals on AMN perfectly match with those computed theoretically, as shown in Fig. 2b.

The same approach was applied to ipso-substitution reactions on AMN. The different symmetry of AMN and toluene was also considered in the scaling of the rate constants of addition and recombination pathways leading to larger PAHs growth. Rate constants tailored from toluene kinetics in the development of AMN mechanism are summarized in Table 1.

Overall, except for the rate constants of the H-atom abstraction by OH from the methyl moiety, discrepancies well below a factor of 2 were obtained between the investigated rate constants for the mono- and di-aromatic hydrocarbon. Hence, the kinetics of unimolecular decomposition and isomerization reactions involving AMN was implemented in analogy with the toluene chemistry from the CRECK kinetic mechanism [14], to which the AMN sub-mechanism was coupled. In doing so, 16 diaromatic hydrocarbon and oxygenated intermediates were added to the kinetic model (see Section 3,2 and Table S1 of SM) in analogy with those primarily involved in toluene combustion. Thermodynamic properties of such species were adopted from Burcat's database [32], when available, or in analogy with structural isomers. The gas-phase mechanism was then coupled to the latest version of the CRECK soot model [31] to account for the formation of large PAHs with >20 C-atoms from AMN combustion, by correcting the kinetics of resonantly stabilized aromatic radical condensation to soot particles from analogous PAH recombination rate constants.

3. Results and discussion

3.1. Laminar flame speed results

Numerical simulations were performed with OpenSMOKE++ [33]. Measured laminar flame speeds of AMN/air mixtures at T_{in}=425 K, 445 K, 484 K are compared with model results in Fig. 3a. The model satisfactorily predicts the flame speed profiles as a function of the equivalence ratio for all the three initial temperatures considered. The highest flame speeds are obtained at φ=1.1, with an increase of 4.6 cm/s from T_{in}=425 K to 445 K and of 9.2 cm/s from T_{in}=445 K to 484 K. Interestingly, similar variations in the maximum LFS were observed in toluene/air combustion at atmospheric conditions [34] with comparable initial temperature difference, i.e., 3.7 and 8.2 cm/s from T_{in}=298 K to 318 K and from T_{in}=318 K to 358 K, respectively. No significant differences in the experimental Markstein lengths could be observed between the three sets (Fig. S5). Fig. 3b compares model predictions at T_{in}=445 K with those of its previous version [14] and of the model proposed by Narayanaswamy et al. [7]. While the former underestimates by ~11 cm/s the experimental data, the latter shows a better quantitative agreement but with peak flame speed shifted towards lower equiv-

Please cite this article as: A. Nobili, L. Pratali Maffei, M. Pelucchi et al., Experimental and kinetic modeling study of α-methylnaphthalene laminar flame speeds, Proceedings of the Combustion Institute, https://doi.org/10.1016/j.proci.2022.08.017

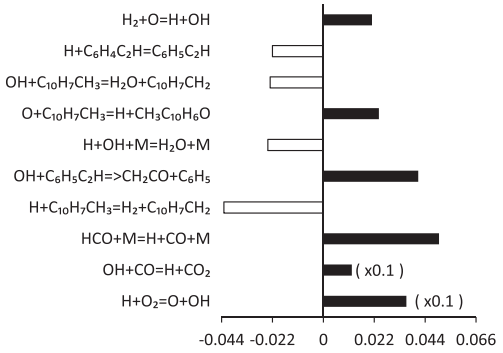

Fig. 4. Sensitivity analysis of LFS to model rate constants for AMN/air flame at T_{in}=445 K, φ=1.1, P=1 bar.

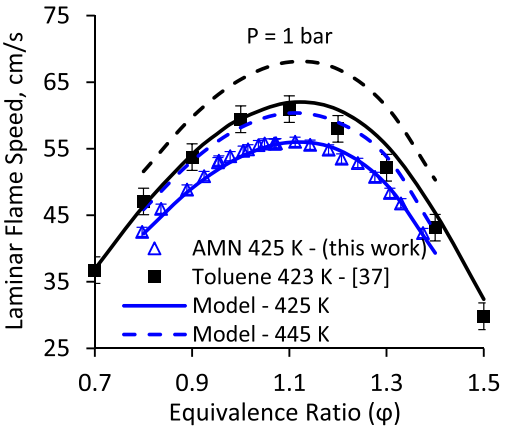

Fig. 5. Comparison between laminar flame speed profile of AMN/air and toluene/air mixtures at T_{in}=425 K and 445 K and P=1 bar. Symbols: experimental data; lines: simulations.

alence ratio than the measured one (i.e., φ=1.05 vs 1.1), and it is also characterized by a larger contribution of fuel unimolecular decomposition reactions to LFS, in both lean and rich conditions, with respect to the here proposed model (see Fig. S9 of the SM). Therefore, this study achieves a significant improvement in the model predictive capability compared to previous literature mechanisms. The model was also tested by comparison with ignition delay times of AMN/air 8,9] and AMN/O_2/Ar [10] mixtures, as well as with speciation of AMN pyrolysis [35] and oxidation [36] from the literature at different operating conditions (P=1-40 bar, T=800-1400 K, φ=0.5-∞), as reported in Table S2 and Figs. S10–S13.

A sensitivity analysis of laminar flame speeds was performed for the case at T_{in}=425 K and φ=1.1. Results from the analysis are reported in Fig. 4. Along with reactions between C_0-C_1 species relevant for H radical formation ($H+O_2=O+OH$, $OH+CO=H+CO_2$, $HCO+M=H+CO+M$), H-atom abstractions by H and OH from the methyl functional group of the fuel govern the reactivity of AMN, as in the case of toluene/air combustion at the same operating conditions (Fig. S8 in SM). Also, phenylacetylene ($C_6H_5C_2H$), primarily produced by the oxidation of two-ring aromatic and oxygenated species (see also Fig. 6), plays a key role. Indeed, its oxidation by OH forming ketene (CH_2CO) and the highly reactive phenyl radical (C_6H_5), compete with H-atom abstraction by OH from AMN, which instead produces a resonantly stabilized radical ($C_{10}H_7CH_2$).

3.2. AMN versus toluene reactivity

Fig. 5 shows the comparison between the simulated LFS profiles of AMN and toluene at atmospheric pressure and for two different initial temperatures, i.e., T_{in}=425 K (solid lines) and T_{in}=445 K (dashed lines). Experimental data by Wang et al. [37] for toluene/air flame speeds at T_{in}=423 K are also reported in comparison with the measurements for AMN/air mixtures from this work. In both model simulations and experiments a higher reactivity of toluene is observed, with a maximum laminar flame speed at φ=1.1 which is ~6 cm/s faster on average than that of AMN in the range of equivalence ratio considered. The reasons behind this difference are explored in the following discussion.

To investigate similarities and differences in the main reaction pathways involved in AMN and toluene combustion, a flux analysis was carried out at T_{in}=445 K and φ=1.1 for both fuels. Results are reported in Fig. 6. In general, mono- and di-aromatic hydrocarbons and oxygenated intermediates with analogous structures are involved in the combustion of toluene and AMN, highlighting the strong correspondence in the kinetics of the two fuels. Specifically, the same five primary intermediates are firstly produced, but with different branching ratios. The reaction flux of AMN towards its radicals, i.e., $C_{10}H_7CH_2$ and $C_{10}H_6CH_3$, is slightly reduced, while those toward naphthalene ($C_{10}H_8$), naphthoxy ($C_{10}H_7O$) and methylnaphthol radical ($OC_{10}H_6CH_3$) are fostered compared to the respective pathways in toluene oxidation. This is primarily due to the H-atom abstraction rate constants from AMN that are different from toluene as discussed in Section 2.2.2.

Decomposition pathways of the two fuel radicals, with the unpaired electron on the methyl group ($C_{10}H_7CH_2$) and the aromatic ring (lumped $C_{10}H_6CH_3$), are highlighted in red and blue, respectively. Ethyl-naphthalene ($C_{10}H_7C_2H_5$) and naphthoquinone ($C_{10}H_6O_2$) species were included in the updated AMN sub-mechanism in analogy with the key intermediates involved in toluene chemistry.

Their inclusion allowed to significantly improve the predictive capability of the model compared to

Please cite this article as: A. Nobili, L. Pratali Maffei, M. Pelucchi et al., Experimental and kinetic modeling study of α-methylnaphthalene laminar flame speeds, Proceedings of the Combustion Institute, https://doi.org/10.1016/j.proci.2022.08.017

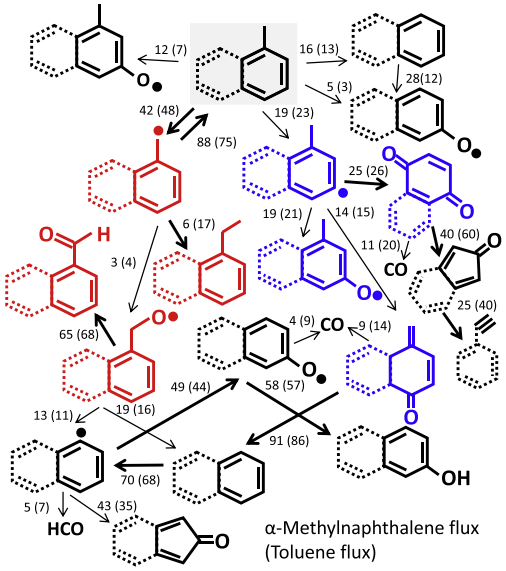

Fig. 6. Comparison between flux analyses of AMN/air and toluene/air combustion at T_{in}=445 K and φ=1.1. The main aromatic intermediates involved in toluene combustion are represented with solid aromatic rings, while those participating to AMN combustion with an additional dashed ring. Thicker arrows represent preferential chemical pathways. Red and blue structures distinguish the pathways originating from methyl group and the ring, respectively.

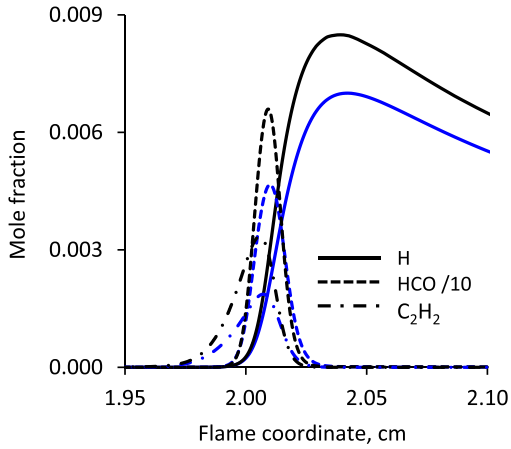

Fig. 7. Simulated mole fraction profiles of H and HCO radicals and acetylene (C_2H_2) in AMN/air (blue lines) and toluene/air (black lines) mixtures at T_{in}=455 K and φ=1.1.

its previous version, as shown in Fig. 3b. In fact, benzoquinone and its two-rings counterpart naphthoquinone ($C_{10}H_6O_2$) are main products of successive reactivity of toluene and AMN aromatic ring radicals, respectively. Their oxidation then produces CO and alkynes, i.e., $C_6H_5C_2H$ and C_2H_2 for AMN and toluene, respectively (Fig. 6). The subsequent oxidation of $C_6H_5C_2H$ was found to be one of the most sensitive reactions for AMN laminar flame speed, as shown in Fig. 4. It can be observed from Fig. 6 that the reaction fluxes of both benzene and phenyl radical in toluene are also similar to those of their two-ring counterparts, corroborating the resembling kinetics of toluene and AMN.

As aforementioned, LFS is strictly related to H radical formation [38]. In particular, the higher LFS of toluene (Fig. 5) is a consequence of the corresponding larger H radical mole fraction with respect to that obtained in the AMN/air mixtures, as also reported in Fig. 7, while the computed adiabatic temperatures of the two flames are comparable (2396 vs 2400 K for toluene and AMN, respectively). This result is expected since toluene features a higher H/C ratio than AMN (1.14 vs 0.91), which leads to larger H radical pool, also considering that a larger fuel mole fraction is required in toluene/air mixtures to reach the same equivalence ratio as AMN/air mixtures (e.g., 0.025 vs 0.017 for φ=1.1, respectively). Fig. 7 also shows that the mole fraction of formyl radical (HCO) and acetylene (C_2H_2), as primary precursors of H radical through HCO+M=H+CO+M and O+C_2H_2=H+HCCO reactions, respectively, is larger in toluene flame, as expected from the decomposition channels of the two fuels reported in Fig. 6.

4. Conclusions

Laminar flame speeds of pure α-methylnaphthalene/air mixtures were measured for the first time in this work. A consolidated spherical vessel apparatus was used for the measurements, performed at 1 bar pressure and three different initial temperatures (T_{in}=425 K, 445 K, and 484 K), with equivalence ratio from 0.8 to 1.35. The AMN kinetic sub-mechanism was updated in analogy with toluene chemistry, exploiting the resembling chemical features of AMN and toluene, and coupled to the CRECK gas-phase and soot models. Rate constant of H-atom abstraction reactions by H, OH and CH_3 radicals from both fuels were computed with theoretical calculations to further assess the validity of the analogy and rate rule approach adopted. It was found that it is reasonable to assume the same rate constants used in toluene kinetics for H-atom abstraction reactions from the methyl functional group of AMN, however the rate constants of the H-atom abstraction by OH was found to be a factor of 1.5 lower than that on toluene. The rate constants of H-atom abstraction reactions from the aromatic rings obtained via rate rules application successfully match the results of the theoretical calculations. Model simulations sat-

Please cite this article as: A. Nobili, L. Pratali Maffei, M. Pelucchi et al., Experimental and kinetic modeling study of α-methylnaphthalene laminar flame speeds, Proceedings of the Combustion Institute, https://doi.org/10.1016/j.proci.2022.08.017

isfactorily predict measured laminar flame speeds in all the conditions experimentally investigated. Flux analyses show the several analogies between the main reaction channels of aromatic and oxygenated intermediates participating in toluene and AMN combustion. On the other hand, it was highlighted that the higher H/C ratio as well the higher concentration of formyl radical and acetylene in the toluene flame, produces a related larger H radical pool, which accelerates the LFS. This largely determines the differences between toluene and AMN, with the latter showing LFS compared to toluene as highlighted by both the experimental measurements and model results.

Declaration of Competing Interest

The authors declare that they have no known competing financial interests or personal relationships that could have appeared to influence the work reported in this paper.

Acknowledgements

This project has received funding from the European Research Council (ERC) under the European Union's Horizon 2020 research and innovation programme (grant agreement n° 756785).

Supplementary materials

SM includes: SM.docx with further details of the experimental apparatus and kinetic model testing. LFS data in tabular form. Kinetic model with species related thermodynamic and transport properties. Input files for MESS calculations.

Supplementary material associated with this article can be found, in the online version, at doi:10.1016/j.proci.2022.08.017.

References

[1] S.M. Sarathy, A. Farooq, G.T. Kalghatgi, Recent progress in gasoline surrogate fuels, Prog. Energy Combust. Sci. 65 (2018) 67–108.
[2] W.J. Pitz, C.J. Mueller, Recent progress in the development of diesel surrogate fuels, Prog. Energy Combust. Sci. 37 (2011) 330–350.
[3] H.P. Ramirez L, K. Hadj-Ali, P. Diévart, G. Moréac, P. Dagaut, Kinetics of oxidation of commercial and surrogate diesel fuels in a jet-stirred reactor: experimental and modeling studies, Energy Fuels 24 (2010) 1668–1676.
[4] A. Violi, S. Yan, E.G. Eddings, A.F. Sarofim, S. Granata, T. Faravelli, E. Ranzi, Experimental formulation and kinetic model for JP-8 surrogate mixtures, Combust. Sci. Technol. 174 (2002) 399–417.
[5] T. Kathrotia, P. Oßwald, J. Zinsmeister, T. Methling, M. Köhler, Combustion kinetics of alternative jet fuels, part-III: fuel modeling and surrogate strategy, Fuel 302 (2021) 120737.
[6] M. Pelucchi, P. Oßwald, W. Pejpichestakul, A. Frassoldati, M. Mehl, On the combustion and sooting behavior of standard and hydro-treated jet fuels: an experimental and modeling study on the compositional effects, Proc. Combust. Inst. 38 (2021) 523–532.
[7] K. Narayanaswamy, G. Blanquart, H. Pitsch, A consistent chemical mechanism for oxidation of substituted aromatic species, Combust. Flame 157 (2010) 1879–1898.
[8] H. Wang, S.J. Warner, M.A. Oehlschlaeger, R. Bounaceur, J. Biet, P.A. Glaude, F. Battin-Leclerc, An experimental and kinetic modeling study of the autoignition of α-methylnaphthalene/air and α-methylnaphthalene/n-decane/air mixtures at elevated pressures, Combust. Flame 157 (2010) 1976–1988.
[9] G. Kukkadapu, C.J. Sung, Autoignition study of 1-methylnaphthalene in a rapid compression machine, Energy Fuels 31 (2017) 854–866.
[10] S. Sun, L. Yu, S. Wang, Y. Mao, X. Lu, Experimental and kinetic modeling study on self-ignition of α-methylnaphthalene in a heated rapid compression machine, Energy Fuels 31 (2017) 11304–11314.
[11] H. Yu, W. Han, J. Santner, X. Gou, C.H. Sohn, Y. Ju, Z. Chen, Radiation-induced uncertainty in laminar flame speed measured from propagating spherical flames, Combust. Flame 161 (2014) 2815–2824.
[12] D. Nativel, M. Pelucchi, A. Frassoldati, A. Comandini, A. Cuoci, E. Ranzi, N. Chaumeix, T. Faravelli, Laminar flame speeds of pentanol isomers: an experimental and modeling study, Combust. Flame 166 (2016) 1–18.
[13] A. Comandini, D. Nativel, N. Chaumeix, Laminar flame speeds and ignition delay times of gasoline/air and gasoline/alcohol/air mixtures: the effects of heavy alcohol compared to light alcohol, Energy Fuels 35 (2021) 14913–14923.
[14] M. Pelucchi, C. Cavallotti, T. Faravelli, S.J. Klippenstein, H-Abstraction reactions by OH, HO_2 , O, O_2 and benzyl radical addition to O_2 and their implications for kinetic modelling of toluene oxidation, Phys. Chem. Chem. Phys. 20 (2018) 10607–10627.
[15] L. Pratali Maffei, M. Pelucchi, C. Cavallotti, A. Bertolino, T. Faravelli, Master equation lumping for multi-well potential energy surfaces: a bridge between *ab initio* based rate constant calculations and large kinetic mechanisms, Chem. Eng. J. 422 (2021) 129954.
[16] A.R. Ghildina, D.P. Porfiriev, V.N. Azyazov, A.M. Mebel, The mechanism and rate constants for oxidation of indenyl radical $C_9 H_7$ with molecular oxygen O_2 : a theoretical study, Phys. Chem. Chem. Phys. 21 (2019) 8915–8924.
[17] L. Pratali Maffei, T. Faravelli, C. Cavallotti, M. Pelucchi, Electronic structure-based rate rules for : H ipso addition-elimination reactions on mono-aromatic hydrocarbons with single and double OH/CH_3 /OCH_3 /CHO/C_2 H_5 substituents: a systematic theoretical investigation †, Phys. Chem. Chem. Phys 22 (2020) 20368–20387.
[18] J.L. Franklin, Mechanisms and kinetics of hydrocarbon combustion, Annu. Rev. Phys. Chem. 18 (1967) 261–282.

Please cite this article as: A. Nobili, L. Pratali Maffei, M. Pelucchi et al., Experimental and kinetic modeling study of α-methylnaphthalene laminar flame speeds, Proceedings of the Combustion Institute, https://doi.org/10.1016/j.proci.2022.08.017

[19] S.J. Klippenstein, From theoretical reaction dynamics to chemical modeling of combustion, Proc. Combust. Inst. 36 (2017) 77–111.
[20] C. Cavallotti, M. Pelucchi, Y. Georgievskii, S.J. Klippenstein, EStokTP: electronic structure to temperature- and pressure-dependent rate constants – a code for automatically predicting the thermal kinetics of reactions, J. Chem. Theory Comput. 15 (2019) 1122–1145.
[21] M. Frisch, G. Trucks, H.B. Schlegel, G.E. Scuseria, M.A. Robb, J.R. Cheeseman, G. Scalmani, V. Barone, Gaussian 09, revision D.01, Gaussian, Inc., Wallingford CT, 2013.
[22] H.J. Werner, P.J. Knowles, F.R. Manby, J.A. Black, K. Doll, A. Heßelmann, D. Kats, A. Köhn, T. Korona, D.A. Kreplin, Q. Ma, Q. Ma, T.F. Miller III, A. Mitrushchenkov, K.A. Peterson, I. Polyak, G. Rauhut, M. Sibaev, The Molpro quantum chemistry package, J. Chem. Phys 152 (2020) 144107.
[23] Y. Georgievskii, J.A. Miller, M.P. Burke, S.J. Klippenstein, Reformulation and solution of the master equation for multiple-well chemical reactions, J. Phys. Chem. A 117 (2013) 12146–12154.
[24] Y. Zhao, D.G. Truhlar, The M06 suite of density functionals for main group thermochemistry, thermochemical kinetics, noncovalent interactions, excited states, and transition elements: two new functionals and systematic testing of four M06-class functionals and 12 other function, Theor. Chem. Acc. 120 (2008) 215–241.
[25] M. Urban, J. Noga, S.J. Cole, R.J. Bartlett, Towards a full CCSDT model for electron correlation, J. Chem. Phys. 83 (1985) 4041–4046.
[26] T.H. Dunning Jr., Gaussian basis sets for use in correlated molecular calculations. I. The atoms boron through neon and hydrogen, J. Chem. Phys. 90 (1989) 1007–1023.
[27] C. Eckart, The penetration of a potential barrier by electrons, Phys. Rev. 35 (1930) 1303–1309.
[28] E. Ranzi, M. Dente, T. Faravelli, G. Pennati, Prediction of kinetic parameters for hydrogen abstraction reactions, Combust. Sci. Technol. 95 (1993) 1–50.
[29] E. Ranzi, C. Cavallotti, A. Cuoci, A. Frassoldati, M. Pelucchi, T. Faravelli, New reaction classes in the kinetic modeling of low temperature oxidation of n-alkanes, Combust. Flame 162 (2015) 1679–1691.
[30] M. Pelucchi, C. Cavallotti, A. Cuoci, T. Faravelli, A. Frassoldati, E. Ranzi, Detailed kinetics of substituted phenolic species in pyrolysis bio-oils, React. Chem. Eng. 4 (2019) 490–506.
[31] A. Nobili, L. Pratali Maffei, A. Baggioli, M. Pelucchi, A. Cuoci, C. Cavallotti, T. Faravelli, On the radical behavior of large polycyclic aromatic hydrocarbons in soot formation and oxidation, Combust. Flame (2021) 111692.
[32] E. Goos, A. Burcat, B. Ruscic, Extended Third Millennium Ideal Gas and Condensed Phase Thermochemical Database for Combustion with Updates from Active Thermochemical Tables. URL = http://garfield.chem.elte.hu/Burcat/THERM.DAT.
[33] A. Cuoci, A. Frassoldati, T. Faravelli, E. Ranzi, OpenSMOKE++: an object-oriented framework for the numerical modeling of reactive systems with detailed kinetic mechanisms, Comput. Phys. Commun. 192 (2015) 237–264.
[34] L. Sileghem, V.A. Alekseev, J. Vancoillie, K.M. Van Geem, E.J.K. Nilsson, S. Verhelst, A.A. Konnov, Laminar burning velocity of gasoline and the gasoline surrogate components iso-octane, n-heptane and toluene, Fuel 112 (2013) 355–365.
[35] H. Jin, J. Hao, J. Yang, J. Guo, Y. Zhang, C. Cao, A. Farooq, Experimental and kinetic modeling study of α-methyl-naphthalene pyrolysis: Part I. Formation of monocyclic aromatics and small species, Combust. Flame 233 (2021) 111587.
[36] K. Mati, A. Ristori, G. Pengloan, P. Dagaut, Oxidation of 1-methylnaphthalene at 1-13 ATM: experimental study in A JSR and detailed chemical kinetic modeling, Combust. Sci. Technol. 179 (2007) 1261–1285.
[37] G. Wang, Y. Li, W. Yuan, Z. Zhou, Y. Wang, Z. Wang, Investigation on laminar burning velocities of benzene, toluene and ethylbenzene up to 20 atm, Combust. Flame 184 (2017) 312–323.
[38] E. Ranzi, A. Frassoldati, R. Grana, A. Cuoci, T. Faravelli, A.P. Kelley, C.K. Law, Hierarchical and comparative kinetic modeling of laminar flame speeds of hydrocarbon and oxygenated fuels, Prog. Energy Combust. Sci. 38 (2012) 468–501.

Please cite this article as: A. Nobili, L. Pratali Maffei, M. Pelucchi et al., Experimental and kinetic modeling study of α-methylnaphthalene laminar flame speeds, Proceedings of the Combustion Institute, https://doi.org/10.1016/j.proci.2022.08.017